Impact of Magnetic Nonlinearities and Cross-Coupling Effects on Properties of Radial Active Magnetic Bearings

Boštjan Polajžer, Gorazd Štumberger, *Member, IEEE*, Jože Ritonja, *Member, IEEE*, Oto Težak, Drago Dolinar, *Senior Member, IEEE*, and Kay Hameyer, *Member, IEEE*

***Abstract*—The impact of magnetic nonlinearities and cross-coupling effects on the properties of the discussed radial active magnetic bearings (AMBs) is evaluated in the entire operating range. The characteristics of flux linkages and radial force are all determined by finite element computation, while the current and position dependent partial derivatives of the flux linkages are calculated by analytical derivations of the continuous approximation functions. Calculated current and position-dependent partial derivatives, as well as the radial force characteristics are incorporated into the proposed dynamic AMB model. The results presented show that the magnetic nonlinearities and cross-coupling effects can change the electromotive forces and the radial force considerably. These disturbing effects have been determined and can be incorporated into the real-time realization of nonlinear control in order to achieve cross-coupling compensations.**

***Index Terms*—Magnetic levitation, modeling, nonlinear magnetics, parameter estimation.**

I. Introduction

ACTIVE magnetic bearings are a system of controlled electromagnets that enable the contact-less suspension of a rotor [1]. Two radial bearings and one axial bearing are used to control the five degrees of freedom of the rotor, while an independent driving motor is used to control the sixth degree of freedom. No friction, no lubrication, precise position control, and vibration damping make active magnetic bearings (AMBs) particularly appropriate and desirable in high-speed rotating machines [2]. Technical applications include compressors, centrifuges, and precise machine tools.

AMBs are a typical electromagnetomechanical coupled system, i.e., the electric and mechanical subsystem are coupled through a magnetic subsystem. The electromagnets of the discussed radial AMBs are placed on the common iron core [3]. Their behavior is, therefore, magnetically nonlinear. Moreover, the individual electromagnets are magnetically coupled, which deteriorate the static and dynamic performances of the overall system. In order to compensate for these disturbing effects, they must be determined in the entire operating range and incorporated into the nonlinear control algorithm.

In this paper, an extended dynamic AMB model is presented, which is appropriate for nonlinear control design and is compact and fast enough for real-time realization. Therefore, a finite element computation-based parametrization coupling model [4] is applied. In the literature, different dynamic AMB models are discussed in terms of parametrization coupling. In [3], the magnetic nonlinearities are taken into account by the nonlinear characteristics of the current gain and position stiffness, while in [5] dynamic inductance is employed along with the nonlinear force characteristic. The electromotive forces (EMFs) due to the cross-coupling effects are neglected in both [3] and [5]. The dynamic AMB model presented in this work is based on the current and position-dependent partial derivatives of flux linkages, as well as on the radial force characteristics, which are determined by the finite-element method (FEM). The magnetic nonlinearities, as well as cross-coupling effects, are therefore considered much more completely than in [3] and [5]. A similar, but experimental-based, approach has already been successfully applied in the modeling and analysis of the linear synchronous reluctance motor [6], [7].

The impact of the magnetic nonlinearities and cross-coupling effects on the properties of the discussed radial AMBs is evaluated by finite-element computation. The radial force characteristic and flux linkages are determined by the two-dimensional (2D) FEM, using the programming environment described in [8]. Calculated force is compared with measured force in the entire operating range, while the flux linkages were not measured due to mechanical problems with rotor fixation. The partial derivatives of the current and position dependent flux linkages are calculated in two steps. In the first, the continuous approximation functions of the FEM-computed flux linkages are determined by differential evolution (DE), a stochastic search algorithm [9]. In the second step, partial derivatives of the continuous approximation functions are calculated analytically. The impact of the magnetic nonlinearities and cross-coupling effects on the radial force and the EMFs of the discussed radial AMBs is then evaluated based on the performed calculations.

Manuscript received July 1, 2003.

B. Polažer, G. Štumberger, J. Ritonja, O. Težak, and D. Dolinar are with the Faculty of Electrical Engineering and Computer Science, Smetanova 17, Maribor SI-2000, Slovenia (e-mail: bostjan.polajzer@uni-mb.si).

K. Hameyer is with the Institute of Electrical Machines, Schinkelstr. 4, Aachen D-52056, Germany.

Digital Object Identifier 10.1109/TMAG.2004.824581

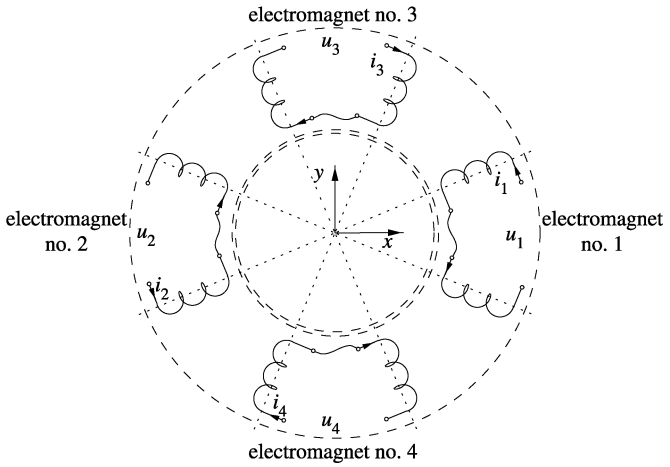

Fig. 1. Circuit AMB model.

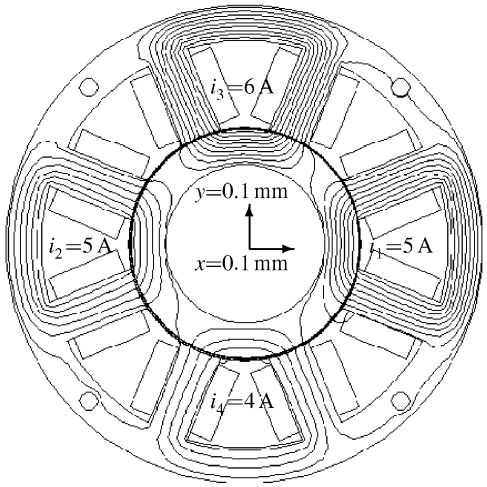

Fig. 2. Geometry and magnetic field distribution of the discussed radial AMBs for the case $x = y = 0.1$ mm, $i_{x\Delta} = 0$ A, $i_{y\Delta} = 1$ A, and $I_0 = 5$ A.

II. Dynamic AMB Model

The dynamic AMB model is according to the circuit model presented in Fig. 1, given by

$$\begin{bmatrix} u_1 \\ u_2 \\ u_3 \\ u_4 \end{bmatrix} = R \begin{bmatrix} I_0 + i_{x\Delta} \\ I_0 - i_{x\Delta} \\ I_0 + i_{y\Delta} \\ I_0 - i_{y\Delta} \end{bmatrix} + 2 \begin{bmatrix} \frac{\partial \psi_1}{\partial i_{x\Delta}} & \frac{\partial \psi_1}{\partial i_{y\Delta}} \\ \frac{\partial \psi_2}{\partial i_{x\Delta}} & \frac{\partial \psi_2}{\partial i_{y\Delta}} \\ \frac{\partial \psi_3}{\partial i_{x\Delta}} & \frac{\partial \psi_3}{\partial i_{y\Delta}} \\ \frac{\partial \psi_4}{\partial i_{x\Delta}} & \frac{\partial \psi_4}{\partial i_{y\Delta}} \end{bmatrix} \begin{bmatrix} \frac{di_{x\Delta}}{dt} \\ \frac{di_{y\Delta}}{dt} \end{bmatrix} + \begin{bmatrix} \frac{\partial \psi_1}{\partial x} & \frac{\partial \psi_1}{\partial y} \\ \frac{\partial \psi_2}{\partial x} & \frac{\partial \psi_2}{\partial y} \\ \frac{\partial \psi_3}{\partial x} & \frac{\partial \psi_3}{\partial y} \\ \frac{\partial \psi_4}{\partial x} & \frac{\partial \psi_4}{\partial y} \end{bmatrix} \begin{bmatrix} \frac{dx}{dt} \\ \frac{dy}{dt} \end{bmatrix} \tag{1}$$

$$\begin{bmatrix} \frac{d^2x}{dt^2} \\ \frac{d^2y}{dt^2} \end{bmatrix} = \frac{1}{m} \begin{bmatrix} F_x(i_{x\Delta}, i_{y\Delta}, x, y) \\ F_y(i_{x\Delta}, i_{y\Delta}, x, y) \end{bmatrix} \tag{2}$$

where u_1, u_2, u_3 and u_4 are the supply voltages, I_0 is the constant bias current, $i_{x\Delta}$ and $i_{y\Delta}$ are the control currents in the x- and in y-axis. ψ_1, ψ_2, ψ_3 and ψ_4 are the flux linkages of the corresponding electromagnets. R stands for the coil resistances. F_x and F_y are the radial force components in the x- and in y-axis, m is the mass of the rotor.

The current and position-dependent partial derivatives of the flux linkages required in (1) are calculated using analytical derivations of the continuous approximation functions of the FEM-computed flux linkages. The force characteristics $F_x(i_{x\Delta}, i_{y\Delta}, x, y)$ and $F_y(i_{x\Delta}, i_{y\Delta}, x, y)$ required in (2) are determined by FEM. In this way, the obtained dynamic AMB model (1), (2) is described in terms of parametrization coupling.

When considering the symmetry in geometry (Fig. 2) and the differential driving mode of currents $i_1 = I_0 + i_{x\Delta}$, $i_2 = I_0 - i_{x\Delta}$, $i_3 = I_0 + i_{y\Delta}$ and $i_4 = I_0 - i_{y\Delta}$, the interaction between electromagnets in the x-axis (no. 1 and no. 2) and electromagnets in the y-axis (no. 3 and no. 4) can be expressed as [10]

$$\begin{aligned} \frac{\partial \psi_1}{\partial i_{x\Delta}} &= \frac{\partial \psi_3}{\partial i_{y\Delta}}, \quad \frac{\partial \psi_1}{\partial i_{y\Delta}} = \frac{\partial \psi_3}{\partial i_{x\Delta}}, \\ \frac{\partial \psi_2}{\partial i_{x\Delta}} &= \frac{\partial \psi_4}{\partial i_{y\Delta}}, \quad \frac{\partial \psi_2}{\partial i_{y\Delta}} = \frac{\partial \psi_4}{\partial i_{x\Delta}} \end{aligned} \tag{3}$$

$$\begin{aligned} \frac{\partial \psi_1}{\partial x} &= -\frac{\partial \psi_2}{\partial x} = \frac{\partial \psi_3}{\partial y} = -\frac{\partial \psi_4}{\partial y}, \\ \frac{\partial \psi_1}{\partial y} &= \frac{\partial \psi_3}{\partial x}, \quad \frac{\partial \psi_2}{\partial y} = \frac{\partial \psi_4}{\partial x}. \end{aligned} \tag{4}$$

The EMFs due to magnetic nonlinearities are reflected in terms such as $(\partial \psi_3 / \partial i_{y\Delta})$ and $(\partial \psi_3 / \partial y)$, which are normally given as constant inductance and speed coefficient, respectively [1]. In [5], magnetic nonlinearities are partially considered with dynamic inductance. However, the EMFs due to cross-coupling effects, which are reflected in terms such as $(\partial \psi_1 / \partial i_{y\Delta})$ and $(\partial \psi_1 / \partial y)$, are neglected in [3] and [5]. The dynamic AMB model (1), (2), therefore, describes the magnetic nonlinearities and cross-coupling effects more completely than similar dynamic models. Furthermore, it is appropriate for nonlinear control design and is compact and fast enough for real-time realization.

III. Finite-Element Computation

The geometry and magnetic field distribution of the discussed radial AMBs is shown in Fig. 2. The problem is formulated by Poisson's equation (5), where $\mathbf{A}$ denotes the magnetic vector potential, ν is the magnetic reluctivity, $\mathbf{J}$ is the current density, and ∇ is Hamilton's differential operator. Magnetostatic computation was performed by 2-D FEM, using the programming environment described in [8]

$$\nabla \cdot (\nu \nabla \mathbf{A}) = -\mathbf{J}. \tag{5}$$

The flux linkage characteristics $\psi_1(i_{x\Delta}, i_{y\Delta}, x, y)$, $\psi_2(i_{x\Delta}, i_{y\Delta}, x, y)$, $\psi_3(i_{x\Delta}, i_{y\Delta}, x, y)$, and $\psi_4(i_{x\Delta}, i_{y\Delta}, x, y)$ were calculated in the entire operating range from the average values of the magnetic vector potential in the stator coils. The radial force characteristics $F_x(i_{x\Delta}, i_{y\Delta}, x, y)$ and $F_y(i_{x\Delta}, i_{y\Delta}, x, y)$ were also calculated in the entire operating range, using two different methods: Maxwell's stress tensor method, where integration was performed over a contour placed along the middle layer of the three-layer air gap mesh, and the virtual work method. The difference between the results obtained by both methods is negligible in the studied case. The

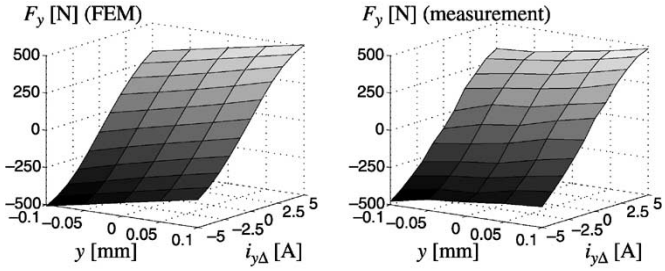

Fig. 3. Radial force characteristic.

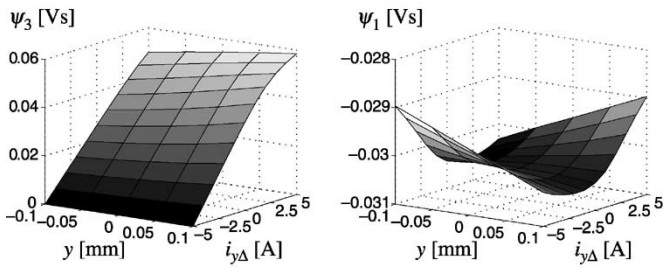

Fig. 4. Flux linkage characteristics calculated by FEM.

obtained results were incorporated into the extended dynamic AMB model (1) and (2). The parametrization coupling model is derived in this way.

IV. Results

The magnetic properties of the rotor surface changed due to the manufacturing process of the rotor steel sheets. Therefore, the magnetic air gap became larger than the geometric one. In order to obtain good agreement between the calculated and measured forces in the linear region, the air gap was increased in FEM computation from 0.4 to 0.45 mm. The 0.05-mm increase in the air gap of can be compared with the findings in [5].

In order to evaluate the impact of the magnetic nonlinearities and cross-coupling effects on the properties of the discussed radial AMBs, it is sufficient to present the results for a case where the control current $i_{x\Delta}$ and the rotor position in the x-axis are equal to zero: $x = 0$ mm, $i_{x\Delta} = 0$ A, and $I_0 = 5$ A.

The good agreement between the FEM-computed and measured radial force characteristics can be seen in Fig. 3. From the obtained results, it is established that the radial force characteristic $F_y(i_{x\Delta} = 0, i_{y\Delta}, x = 0, y)$ is linear inside the expected operating range ($i_{y\Delta} \in [-2\text{ A}, 2\text{ A}]$, $y \in [-0.1\text{ mm}, 0.1\text{ mm}]$) [10]. Furthermore, due to the control current $i_{x\Delta}$ and the rotor position in the x-axis, the radial force component F_y can vary in a range of up to 13%.

In Fig. 4, FEM-based results are given for the flux linkage characteristics. They were not compared to the measured ones because the flux linkages were not measured due to mechanical problems with rotor fixation.

Results of finite-element computation $\psi_3(i_{y\Delta}, y)$ and $\psi_1(i_{y\Delta}, y)$ are presented analytically by (6), where f is a continuous approximation function of two variables, u and v. The parameters d_{ij} ($i = 1,\ldots,4$; $j = 1,\ldots,4$) were determined by DE [9]. Obtained parameters are presented in matrix form by (7) for the approximation of $\psi_3(i_{y\Delta}, y)$ and by (8) for the approximation of $\psi_1(i_{y\Delta}, y)$. The agreement is excellent between the FEM-computed flux linkages and the flux linkages calculated by corresponding continuous approximation functions. Inside the expected operating range ($i_{y\Delta} \in [-2\text{ A}, 2\text{ A}]$, $y \in [-0.1\text{ mm}, 0.1\text{ mm}]$) the relative difference $(\psi_{(\cdot)}^{(\mathrm{FEM})} - \psi_{(\cdot)}^{(\mathrm{approx})})/\psi_{(\cdot)}^{(\mathrm{FEM})}$ is calculated, where $\psi_{(\cdot)}^{(\mathrm{FEM})}$ are FEM-computed flux linkages, while $\psi_{(\cdot)}^{(\mathrm{approx})}$ are corresponding continuous approximation functions. The obtained maximum relative difference is 2.66% for $\psi_3(i_{y\Delta}, y)$ and 0.25% for $\psi_1(i_{y\Delta}, y)$, as shown in (6)–(8) at the bottom of the page.

The current and position-dependent partial derivatives of flux linkages were calculated by analytical derivations of the corresponding continuous approximation functions. The analytical derivations of the continuous approximation functions are justified for the studied case. Based on a comparison between the results of the proposed analytical derivations (Figs. 5 and 6), as well as the results of the numerical derivations [10], a maximum relative difference of 25% is established.

In the results shown in Fig. 5, it can be seen that the current and position-dependent partial derivatives of the flux linkage in the y-axis are not constant, which indicates the influence of magnetic nonlinearities. The influence of magnetic cross-coupling effects can be seen in the results shown in Fig. 6, since the current and position-dependent partial derivatives of the flux linkage in the x-axis are not zero. The impact of the magnetic nonlinearities and cross coupling effects on the EMFs was analyzed based on the obtained results. Therefore, the ratio $(\partial\psi_1/\partial i_{y\Delta})/(\partial\psi_3/\partial i_{y\Delta})$,

$$f(u,v) = (d_{33}e^{-d_{31}v} + d_{34}e^{-d_{32}v})e^{-(d_{13}e^{-d_{11}v} + d_{14}e^{-d_{12}v})u} + (d_{43}e^{-d_{41}v} + d_{44}e^{-d_{42}v})e^{-(d_{23}e^{-d_{21}v} + d_{24}e^{-d_{22}v})u} \tag{6}$$

$$[d_{ij}] = \begin{bmatrix} -4.310\,445 & -4.310\,500 & -1540.657\,786 & 1540.681\,058 \\ -4.208\,488 & -4.208\,603 & -792.059\,338 & 792.074\,968 \\ 2.103\,857 & -4.423\,200 & -0.775\,770 & -0.019\,074 \\ -4.067\,947 & 2.077\,838 & 0.035\,394 & 0.789\,790 \end{bmatrix} \tag{7}$$

$$[d_{ij}] = \begin{bmatrix} 1.714\,112 & -6.907\,251 & -0.044\,694 & -0.003\,038 \\ -6.133\,745 & 1.839\,766 & -0.002\,791 & -0.037\,607 \\ -0.668\,224 & -0.227\,556 & 0.019\,102 & 0.145\,872 \\ -4.875\,218 & -0.221\,698 & -0.000\,530 & -0.194\,783 \end{bmatrix} \tag{8}$$

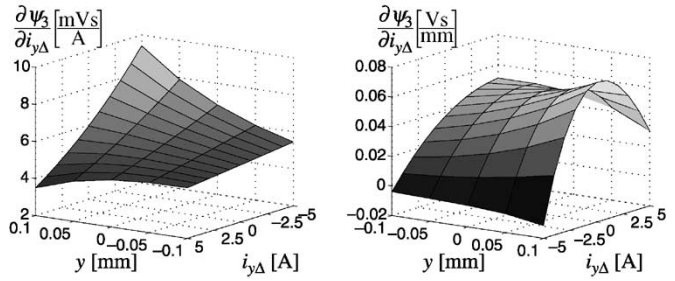

Fig. 5. Analytically calculated flux linkage partial derivatives in the y-axis.

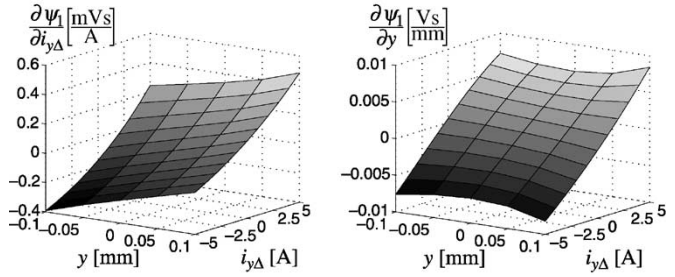

Fig. 6. Analytically calculated flux linkage partial derivatives in the x-axis.

as well as the ratio $(\partial\psi_1/\partial y)/(\partial\psi_3/\partial y)$, was calculated inside the expected operating range ($i_{y\Delta} \in [-2\text{ A}, 2\text{ A}]$, $y \in [-0.1\text{ mm}, 0.1\text{ mm}]$). The obtained maximum values are 0.05 for $(\partial\psi_1/\partial i_{y\Delta})/(\partial\psi_3/\partial i_{y\Delta})$ and 0.12 for $(\partial\psi_1/\partial y)/(\partial\psi_3/\partial y)$. From the performed comparison, it is established, that due to magnetic nonlinearities and cross-coupling effects, the EMFs can vary in a range of up to 12%. Furthermore, when considering the maximum current slew rate (240 A/s) and the maximum position slew rate (0.012 m/s), a dominant influence of the EMFs due to current change can be expected.

V. Conclusion

The impact of magnetic nonlinearities and cross-coupling effects on the properties of the discussed radial AMBs is studied in this paper. For this purpose, an analysis of current and position-dependent flux linkages and radial force characteristics was performed by FEM computation and analytical derivations of the continuous approximation functions. The results of the performed calculations have been incorporated into the proposed dynamic AMB model. The parametrization coupling model of the discussed radial AMBs is derived in this way. It has been shown that the dynamic AMB model presented in this work considers the magnetic nonlinearities, as well as cross-coupling effects, much more completely than similar models. The presented results show that the influence of magnetic nonlinearities and cross-coupling effects is significant. Inside the expected operating range of the discussed radial AMBs, the EMFs can vary due to the magnetic nonlinearities and cross-coupling effects in a range of up to 12%, while the radial force can vary in a range of up to 13%. These disturbing effects deteriorate the static and dynamic performances of the overall system. In order to improve the system dynamics, the obtained results have to be incorporated into real-time realization of nonlinear control. In this way, direct compensation can be achieved for the magnetic nonlinearities and cross-coupling effects.

References

[1] G. Schweitzer, H. Bleuler, and A. Traxler, "Active Magnetic Bearings," *ETH Zürich: Vdf Hochschulverlag AG an der ETH Zürich*, 1994.

[2] R. Larsonneur, "Design and Control of Active Magnetic Bearings Systems for High Speed Rotation," Ph.D. dissertation, ETH Zürich, Zürich, Switzerland, 1990.

[3] G. Štumberger, D. Dolinar, U. Pahner, and K. Hameyer, "Optimization of radial active magnetic bearings using the finite element technique and the differential evolution algorithm," *IEEE Trans. Magn.*, vol. 36, pp. 1009–1013, July 2000.

[4] K. Srairi and M. Féliachi, "Numerical coupling models for analyzing dynamic behaviors of electromagnetic actuators," *IEEE Trans. Magn.*, vol. 34, pp. 3608–3611, Sept. 1998.

[5] M. Antila, E. Lantto, and A. Arkkio, "Determination of forces and linearized parameters of radial active magnetic bearings by finite element technique," *IEEE Trans. Magn.*, vol. 34, pp. 684–694, May 1998.

[6] G. Štumberger, B. Štumberger, and D. Dolinar, "Magnetically nonlinear and anisotropic core model of synchronous reluctance motor," *J. Magnetism Magn. Materials*, vol. 254/255, pp. 618–620, 2003.

[7] ——, "Position and current dependent flux linkages, thrust and friction force of linear synchronous reluctance motor," in *Proc. 36th IAS Annual Meeting*, 2001, pp. 2310–2317.

[8] U. Pahner, R. Mertens, H. De Gersem, R. Belmans, and K. Hameyer, "A parametric finite element environment tuned for numerical optimization," *IEEE Trans. Magn.*, vol. 34, pp. 2936–2939, Sept. 1998.

[9] O. Težak, G. Štumberger, B. Polažer, and D. Dolinar, "Advanced methods in surface approximation," in *Proc. 14th Int. Conf. Systems Research, Informatics and Cybernetics*, 2002, pp. 20–24.

[10] B. Polajžer, "Design and Analysis of an Active Magnetic Bearing Experimental System," Ph.D. dissertation, Faculty of Electrical Engineering and Computer Science, University of Maribor, Maribor, Slovenia, 2002.